

## RESEARCH ARTICLE

# New Graphene-Based on Nickel-Carbon Compounding Applied to Carbon Brushes of Traction Motors in Subway Vehicles

LIANG-YIN HUANG<sup>1</sup>, SHIUE-DER LU<sup>2</sup>, (Member, IEEE), AND HWA-DONG LIU<sup>3</sup>

<sup>1</sup>Graduate Institute of Manufacturing Technology, National Taipei University of Technology, Taipei 106, Taiwan

<sup>2</sup>Department of Electrical Engineering, National Chin-Yi University of Technology, Taichung 411, Taiwan

<sup>3</sup>Undergraduate Program of Vehicle and Energy Engineering, National Taiwan Normal University, Taipei 106, Taiwan

Corresponding author: Hwa-Dong Liu (hdlu@ntnu.edu.tw)

This work was supported in part by the National Science and Technology Council, Taiwan, under Grant MOST 112-2221-E-003-003; in part by the National Taiwan Normal University Subsidy Policy for International Collaboration and Research Projects; in part by the National Taiwan University of Science and Technology (NTUS) Innovation Cooperation under Grant 11212151003; and in part by the National Taiwan Normal University (NTNU), Taiwan.

**ABSTRACT** This study developed a novel graphene process technology based on nickel-carbon compounding. This process can be applied to carbon brushes of traction motors in subway vehicles. We heated nickel metal to 1000 °C, and multilayer graphene film was deposited over a large area. The graphene-based nickel carbon (GBNC) was tested using an energy dispersive spectrometer (EDS) and Raman spectrometer, with a G peak of 1580 cm<sup>-1</sup> and a 2D peak of 2750 cm<sup>-1</sup>. The peak intensities were 2887 cm<sup>-1</sup> and 2275 cm<sup>-1</sup>, respectively. The findings verified that graphene produced using the nickel-carbon compounding process technology has typical graphene characteristics. A GBNC carbon brush was installed on a traction motor during the actual measurement. The proposed GBNC carbon brush cost was 20 % lower than the traditional graphite carbon brush. Moreover, the wear loss was 30 % lower. The findings suggest that the graphene performance is superior to traditional graphite carbon brushes regarding conducting efficiency, thermal conductivity, and lubricating properties. Therefore, the GBNC carbon brush proposed in this study has good performance. The GBNC carbon brush failure rate is lower than the traditional graphite carbon brush. Using the GBNC carbon brush enhances traction motor stability. It also reduces maintenance costs, which improves the efficiency of the electric multiple unit (EMU) propulsion systems to enhance the subway company's service quality, equipment quality, and corporate image.


**INDEX TERMS** Graphene-based nickel carbon, graphite, electric multiple units, traction motor, subway vehicles.

## I. INTRODUCTION

Graphite is a planar, laminar material composed of carbon and is classified as an allotrope. Three electronic structures surround a carbon atom, forming a mixed region with peripheral carbon atoms (3), where a hexahedral cubic lattice structure occurs. The distance of each carbon atom is 0.142 nm. The Van der Waals force attracts the graphite layers, and the primary spacing is approximately 0.34 nm. One valence electron exists, making the graphite a conductive material. Graphite is a crystalline nonmetal material with high-temperature

resistance, good conductivity, and excellent lubrication. It is widely used in various industrial fields, such as petrochemicals [1], [2], machinery [3], [4], electric appliances [5], [6], [7], [8], [9], aerospace [10], medical treatments [11], [12], [13], [14], national defense [15], and solar energy [16].

According to the energy dispersive spectrometer (EDS) composition analysis, the commercially available general carbon brush contains carbon, copper, lead, tin, and iron [17]. However, its poor durability results in considerable wear, which can increase maintenance costs. Graphene and nickel, with representative superiority, were selected for this study, considering the material characteristics. Their superior physical properties [18] include high mechanical stress,

The associate editor coordinating the review of this manuscript and approving it for publication was Amin Mahmoudi .

high thermal conductivity, a highly directional surface, wear-lubricating properties, and high electron mobility. These can all increase electrical conduction efficiency. Therefore, this study used graphene-based nickel carbon (GBNC) as the traction motor carbon brush material.

There are several methods for producing graphene materials [19], [20], [21], [22], [23], [24], [25]. Mazurek et al. discussed the influence of graphene deposition on the copper electrode emission spectrum. Graphene was obtained using chemical vapor deposition for electronic devices [19]. Sun developed a photochemical reduction-oxidation graphene, where the light dosage controlled the degree of oxidation-reduction. The obtained graphene had high quality and excellent conductivity, suitable for fuel cell electrode devices [20]. Xia et al. separated graphene and metal structures through a thin organic dielectric layer for THz modulators [21]. Li et al. used Ge-enhanced chemical vapor deposition to grow graphene, which had high conductivity and was applied to gas sensors [22]. Xia et al. developed a technology using a laser to generate graphene. The grown graphene was three-dimensional and applicable to sensor devices [23]. Yu et al. combined heterogeneous materials based on multilayer graphene technology. They found that the material enhanced the photoelectric properties and had a faster reaction rate [24]. Chen et al. covered a metal surface with oxidized graphene to detect the glucose in human blood with good accuracy [25].

The present study used graphene as a carbon brush in traction motors of subway vehicles due to the excellent physical characteristics of graphene carbon brushes [26]. It has high-temperature resistance, exceptional thermal performance, excellent electrical and thermal conductivity, lubricating properties, plasticity, and chemical stability. This study found that the GBNC carbon brush has good performance. Furthermore, the carbon brush is an essential component for conducting current between the rotating and stationary parts of a traction motor, which can effectively reduce traction motor failure rates. The GBNC carbon brush enhances traction motor stability, lowers maintenance costs, and improves electric multiple unit (EMU) operating quality.

TABLE 1 shows a comparison of carbon brushes of different materials. First, compare three materials of carbon brushes, namely copper carbon, stainless steel, and nickel carbon. Second, [27] and [28] materials are both copper carbon, but their copper amount is 10 % and 50 %, respectively, so the characteristic is different. Finally, the proposed GBNC generates graphene and it has good conducting efficiency and wear resistance. The GBNC conducting efficiency and wear resistance are better than other carbon brushes [27], [28], [29].

This paper has been categorized into five sections. The introduction has been discussed in section I. Introducing the subway vehicle propulsion system has been discussed in section II. Novel GBNC technology has been presented in section III. Experimental results are detailed in section IV, and the conclusion is presented in the final section.

TABLE 1. Comparison of different materials' carbon brushes.

Carbon brush	Material	Conducting efficiency	Wear resistance
[27]	Copper-carbon	Medium	Medium
[28]	Copper-carbon	Good	Medium
[29]	Stainless steel	Medium	Medium
GBNC	Nickel-carbon	Good	Good

## II. INTRODUCING THE SUBWAY VEHICLE PROPULSION SYSTEM

Subway vehicle propulsion systems are installed in power cars to provide driving power. Figure 1 shows the circuit architecture of a power propulsion system, where TM1, TM2, TM3, and TM4 represent the four traction motors of a power car. The variable voltage variable frequency (VVVF) describes the traction inverter and provides electricity for the traction motor.

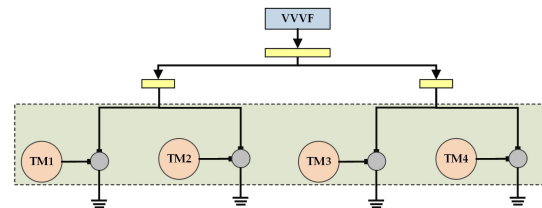
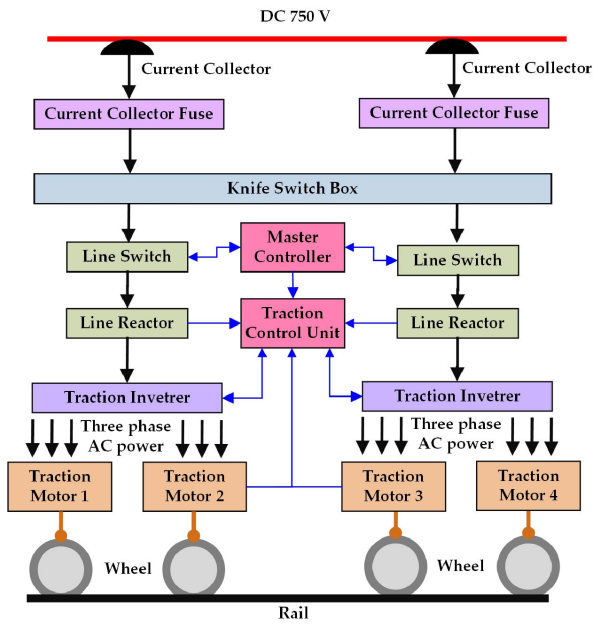


FIGURE 1. Circuit architecture diagram of a power propulsion system for subway vehicles.

The propulsion system signals when the EMU master controller or driver issues a control command. The signal is converted into a pulse width modulation (PWM) signal, and the traction inverter converts the direct current (DC) 750 V electricity into a three-phase alternating current (AC). The propulsion system operates the traction motor and provides power for the EMU. If the master controller or driver issues a deceleration command, the traction inverter exports a lower amount of AC to reduce the operating speed of the traction motor. Additionally, the traction motor operates with inertia when a train is coasting. It turns into a generator and exports electricity, which is fed back to the third rail. If the feedback voltage exceeds 900 V, the EMU brake resistor is actuated, the feedback voltage is reduced, and the subway company's power system is protected.

Figure 2 shows the electric control structure diagram of a power car propulsion system for subway vehicles. First, the third rail provides a voltage of 750 V, and the power car's current collector receives the electric power. Next, the 750 V power is transmitted to the line switch and reactor through the knife switch box and current collector fuse. Finally, the 750 V power is transmitted to the traction inverter. The three-phase AC is exported to drive the traction motor, the traction motor rotates the gearbox to operate the wheels, and the EMU moves forward. The master controller instructs the traction control unit to regulate the three-phase AC exported from



**FIGURE 2.** Electric control structure diagram of a power car propulsion system.

the traction inverter. The master control regulates the traction motors to accelerate/decelerate the EMU in a timely manner.

The electric control structure diagram of a power car propulsion system for subway vehicles is shown in Figure 2. Figure 3 illustrates the essential components of a power car propulsion system, including the current collector, as shown in Figure 3 (a). Figure 3 (b) illustrates the knife switch box. Figure 3 (c) shows the line switch and electrical equipment boxes. Figure 3 (d) shows the traction motor. Figure 3 (e) shows the wheel. Figure 3 (f) shows the master controller. Figure 3 (g) represents the line reactor. These components comprise relevant power circuits of a propulsion system (see Figures 2 and 3) in building a propulsion system.

This study developed a novel graphene-based nickel-carbon compounding method and applied it to the carbon brush of traction motors in a propulsion system for subway vehicles. The traction motor carbon brush is essential for conducting current between rotating and stationary parts. However, the carbon brush may be damaged in actual operation due to high current, long run time, and other effects. As such, this study developed a GBNC carbon brush due to its good electrical conductivity and excellent wear resistance. The developed GBNC carbon brush was installed in a traction motor for actual operation and was analyzed and compared to the traditional graphite carbon brush.

### III. NOVEL GBNC TECHNOLOGY

#### A. GBNC

Figure 4 illustrates the graphene-based nickel carbon (GBNC) production process. First, physical vapor deposition coated a nickel film on a carbon block. The substrate's diameter was 5 mm, and its height was 1 mm. After adjusting the

nickel-carbon ratio and heat treatment, the nickel film was sputtered onto the graphite block substrate surface for 30 minutes to form a graphene film on the metal surface. Since the nickel of the metal film is a catalyst, a steadier lattice structure can be resynthesized under the catalyst effect. This principle significantly increases the graphene film formation rate. Furthermore, this study observed the formation and characteristics of the graphene film at the heating condition (1000 °C). The separated graphene film can be applied to circuit laying and electronic modules, which can meet various applications in the future. In the present study, graphite powder was compressed into an ingot with an oil pressure unit before using the natural carbon powder (K23) for growing graphene. The ingot was the substrate, and the nickel film was coated on the ingot surface through sputtering. It was adjusted and sintered by vacuum degree and inert gases for about one hour, which ensured that the carbon atoms were diffused and deposited on the transition metal film of the graphite ingot. The graphene film (silver) was formed on the ingot surface. Then, the graphene film's morphology and characteristics were observed. Finally, the characteristics of the graphene grown based on nickel-carbon compounding were tested using an energy dispersive spectrometer (EDS) and a Raman spectrometer.

This study produced the graphene was using a sputtering system with physical vapor deposition. The nickel and carbon elements were insoluble for lattice mismatch. The melting point of nickel is 1455 °C, whereas the melting point of the carbon element is 3827 °C, which influences the graphite layer's continuity. This study used nickel metal as a catalyst, and the carbon atoms were diffused and separated from the nickel. A hexagonal annular crystalline film was formed to obtain a large, smooth graphite layer. Adding Ni element enhanced the strength of graphite film and increased the film's deposition.

A radio frequency source (13.56 MHz) negatively charges the insulating material. Electrons are accelerated through high-frequency electric field variation. Gas molecules are ionized, resulting in a glow effect. With gas flow, ions react with atoms to form atomic groups. Then, the atomic groups react with the ions to form particles, and the particles deposit to create a film.

Regarding the sputtering method, the vacuum degree  $7 \times 10^{-3}$  torr was achieved using a mechanical pump. The vacuum degree  $3 \times 10^{-6}$  torr was achieved using a diffusion pump. Thus, a uniform, pure film was deposited in a high vacuum. The power was regulated with a load voltage for optimal particle deposition density.

Figure 5 shows the schematic diagram of the gun body model. The gun body was vacuumed to a fixed value using a vacuum machine for actuation. Next, argon gas was supplied. The carbon rod received a continual spread of inert gas, and the nickel sputtering effect was applied to the glow effect area. The power modulation was confirmed in this process. The sputtering glow variation was observed through the transparent window outside the gun body. The power value was



**FIGURE 3.** Essential components of a power car propulsion system: (a) current collector, (b) knife switch box, (c) line switch box and electrical equipment box, (d) traction motor, (e) wheel, (f) master controller, (g) line reactor.

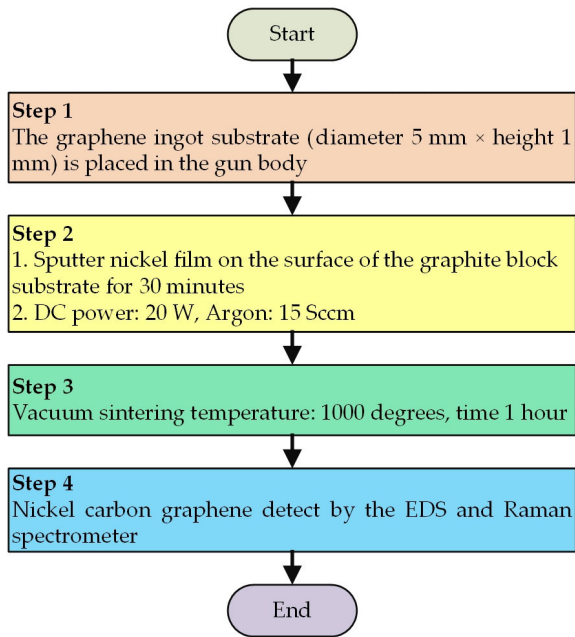


FIGURE 4. The GBNC production process.

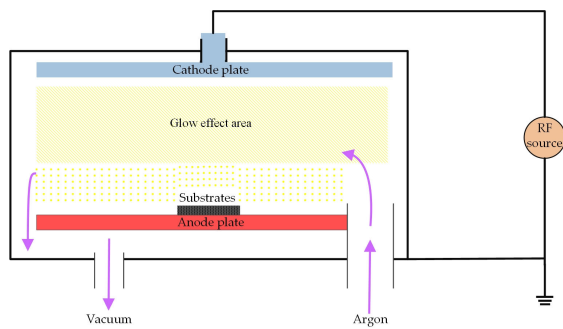


FIGURE 5. Schematic diagram of the gun body model.

fixed after determining the argon volume. The time was at least 30 minutes, and the duration was determined according to the results of 3 to 5 tests.

The ideal graphene film load factor computing mode was based on experience operating a transmission electron microscope (TEM). The density and thickness-related values on the graphene film can be expressed as the following equation to calculate the graphene film load factor:

$$W_k = \frac{N_{w1}f_s L_p}{N_{w2}B_s} Q_s \quad (1)$$

where  $W_k$  is the load factor of the graphene film deposited after nickel and carbon sputtering,  $Q_s$  is the mol ratio carrier of surface atoms,  $L_p$  is the average atom content of graphene,  $B_s$  is the area density,  $N_{w1}$  is the molecular weight of graphene atoms,  $N_{w2}$  is the molecular weight of the carrier atoms, and  $f_s$  represents the graphene. The nickel and carbon sputtering on the graphene film favor formed uniform graphene film with several layers on the carrier surface. TABLE 2 shows the nickel-carbon compounding specifications for graphene.

TABLE 2. Nickel-carbon compounding specification sheet for the graphene.

Item/name	Specification/parameter
Ingot substrate	Natural carbon powder (K23)
Ingot size	Diameter 5 mm × height 1 mm
Sputtering material	Nickel
Sputtering power	20W
Argon supply	15 Sccm
Vacuum sintering heat treatment furnace temperature	1000 °C
Retention time	At least 30min~1hr

### B. ANALYSIS OF GRAPHENE OF NICKEL CARBON COMPOUNDING

Figure 6 shows the nickel metal deposited at 20 W power and a magnification of 100 times observed through an energy dispersive spectrometer (EDS). The carbon atoms were adsorbed on the nickel film’s surface. The nickel film had a face-centered cubic (FCC) structure. Over time, the amorphous carbon atoms grew with nearby graphite film along the nickel film, producing a large-area graphene film. The nickel and graphite generated thermal stress during cooling due to different thermal expansion coefficients. The graphite film on the nickel film’s surface grew several stacked wrinkles. According to the observation through EDS, the carbon atoms were adsorbed on the surface of the transition metal, which was diffused and separated from the transition metal film’s surface. The graphite flaked aggregate under the catalysis of the transition metal at high temperatures to form a relatively smooth graphene film.

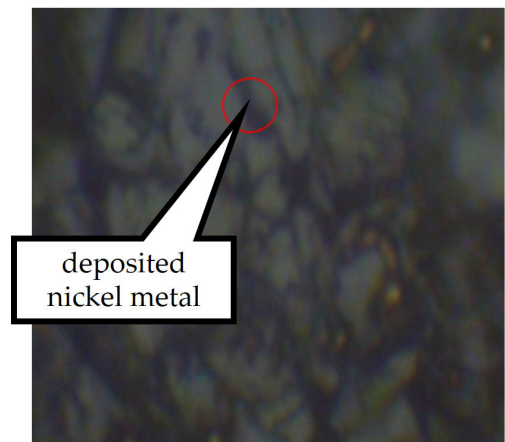
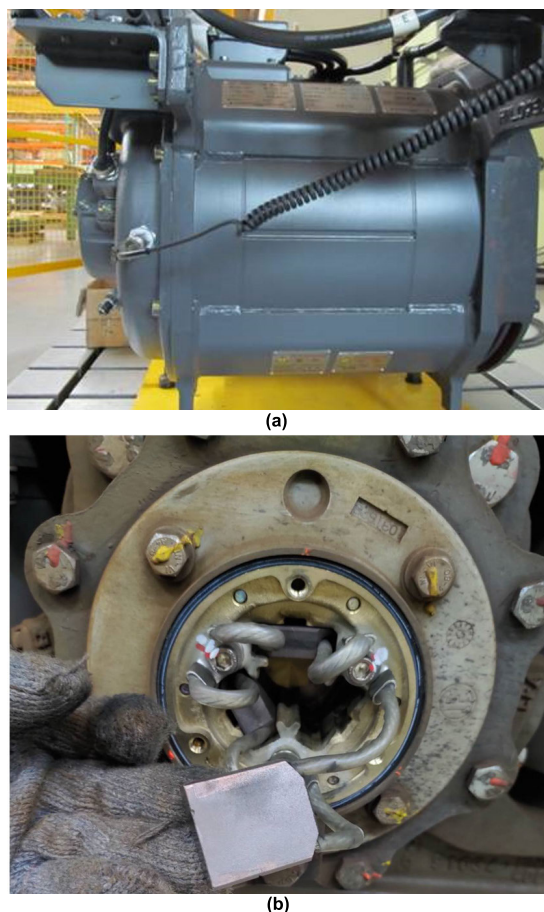


FIGURE 6. Nickel metal deposited at a power of 20 W (magnified 100 times).

### IV. EXPERIMENTAL RESULTS

Figure 7 shows this study’s stereogram of the propulsion system traction motor. Figure 7 (a) represents the side view of the traction motor. Figure 7 (b) displays the traction motor carbon brush.

Figure 8 displays the graphene film based on nickel carbon at a temperature of 1000 °C production with the EDS. Fig. 8 (a) is magnified ×1000 times. Figure 8 (b) is magnified at ×2000 times. Fig. 8 (c) is magnified at ×7000 times.

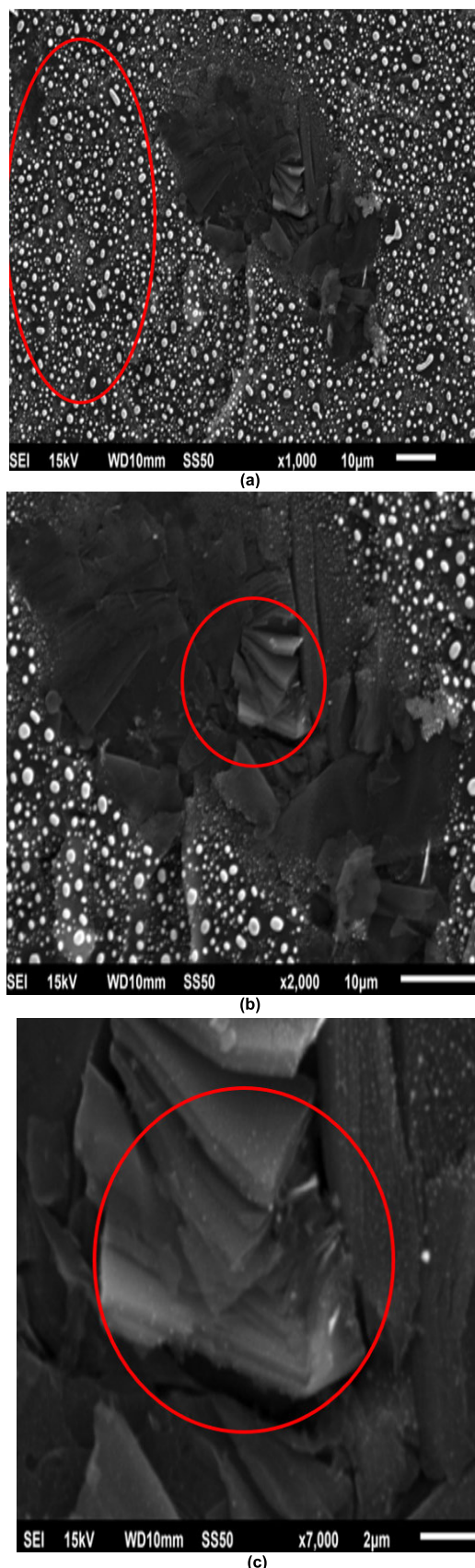


**FIGURE 7.** Stereogram of the propulsion system of a traction motor: (a) side view of a traction motor, (b) traction motor carbon brush.

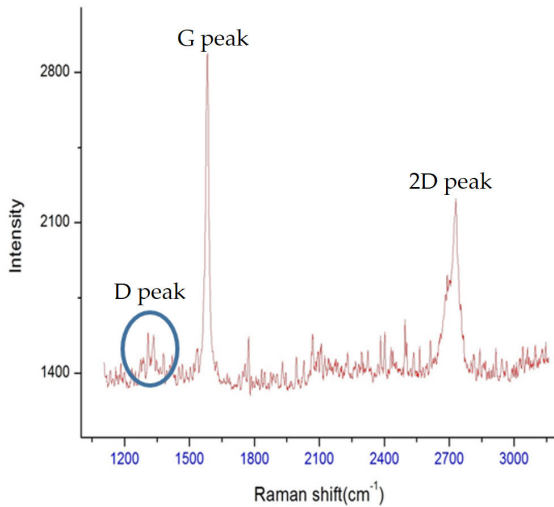
Figures 8 (a), (b), and (c) show how the nickel-carbon sputtering deposited a multilayer graphene film based on nickel carbon. Nickel carbon has a good catalytic capability for graphite. The graphite deposited on the transition nickel metal surface was flaky and stacked in a small area because the nickel (111) and carbon (0001) had a good lattice match.

Figure 9 shows the graphene film based on nickel carbon at a temperature of 1000 °C production using a Raman spectrometer. There was no significant D peak (defect peak) at 1350  $\text{cm}^{-1}$ . The peak intensity was about 1575  $\text{cm}^{-1}$ . At 1580  $\text{cm}^{-1}$  (G band) and 2700  $\text{cm}^{-1}$  (2D band), the peak intensities were 2887  $\text{cm}^{-1}$  and 2275  $\text{cm}^{-1}$ , respectively. Therefore, the traction motor carbon brush prepared in this study has the graphene feature. The G band intensity was about 2887  $\text{cm}^{-1}$ . There were few layers, the 2D band intensity was about 2275  $\text{cm}^{-1}$ , and the relative ratio was about 0.79.

Figure 10 shows the graphene film based on graphite at a temperature of 1000 °C production using a Raman spectrometer. There is an obvious D peak at the position of 1350  $\text{cm}^{-1}$ . Its intensity is relatively high compared with Figure 9, which indicates that there are more defects and there may be more wrinkles and the formation of a graphite film with a larger



**FIGURE 8.** The graphene film based on nickel carbon from a temperature of 1000 °C production with the EDS: (a)  $\times 1000$  times, (b)  $\times 2000$  times, and (c)  $\times 7000$  times.



**FIGURE 9.** The graphene film based on nickel carbon from a temperature of 1000 °C production with a Raman spectrometer.

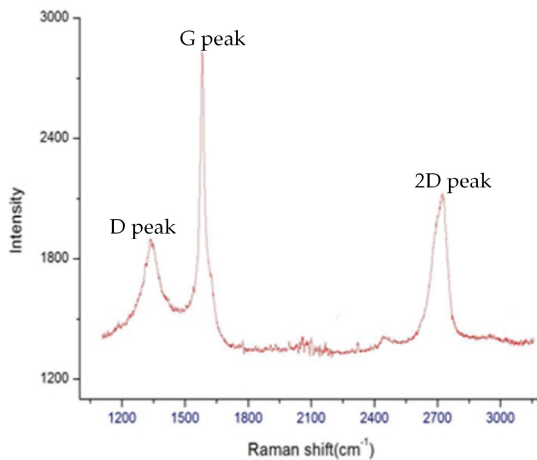


**FIGURE 10.** The graphene film based on graphite from a temperature of 1000 °C production with a Raman spectrometer.

number of layers. If there is a product, its quality is relatively poor.

TABLE 3 compares the experimental features of the GBNC carbon brush and traditional graphite carbon brush. The unit price of the GBNC carbon brush is 68.6 USD, which is more cost-effective than the traditional graphite carbon brush. The wear loss of the GBNC carbon brush is 2.1 mm/year, lower than that of the traditional graphite carbon brush. Additionally, the GBNC carbon brush performs better than the traditional graphite carbon brush in terms of conducting efficiency, thermal conductivity, and lubricating properties.

TABLE 4 shows the comparison table of the failure data of the GBNC and traditional graphite carbon brushes. There are a total of 272 traction motors in 17 trains of the subway company’s yellow line. According to statistics, 28 cases of traditional graphite carbon brushes failed (failure rate of 10.3 %). The 272 traction motors were replaced with GBNC carbon brushes and 3 cases failed (failure rate of 1.1 %). The GBNC and traditional graphite carbon brushes usage

**TABLE 3.** Comparison table of the experimental features of the GBNC and traditional graphite carbon brushes.

Carbon brush type	Unit price (US D)	Wear loss (mm/yea r)	Conducti ng efficiency	Thermal conductivi ty	Lubricati ng property
GBNC	68.6	2.1	Good	Good	Good
Tradition al graphite	85.7	3	Normal	Normal	Normal

**TABLE 4.** Comparison table of the failure data of the GBNC and traditional graphite carbon brushes.

Carbon brush type	Failure amount	Failure rate	Usage time
GBNC	3	1.1 %	6 years
Traditional graphite	28	10.3 %	3 years

time is 6 years and 3 years, respectively. Therefore, the proposed GBNC carbon brush has better stability and safety.

### V. CONCLUSION

This study developed a novel graphene process technology based on nickel-carbon compounding. The GBNC was tested using EDS and Raman spectrometers, proving its graphene characteristics. It was also applied to the carbon brush of a traction motor in a subway vehicle propulsion system. The cost of the GBNC carbon brush was 20 % lower than the traditional graphite carbon brush. The wear loss was reduced by 30 %. It has good wear resistance, conducting efficiency, thermal conductivity, and lubricating properties. The GBNC carbon brush failure rate of 1.1 % is lower than the traditional graphite carbon brush failure rate of 10.3 %. The proposed GBNC carbon brush effectively reduces the traction motor failure rate, enhances stability and vehicle safety, and reduces maintenance costs.

The GBNC material can be applied to high-speed rail or electric vehicle traction motors to maintain public traffic stability and reduce maintenance costs. Moreover, graphene with better performance can be developed for vehicles, industrial electronics, and medical electronics in the future.

### REFERENCES

- [1] A. Shadab and S. K. Raghuvanshi, “Development and sensitivity analysis of rGO-TiO<sub>2</sub> coated eFBG sensor for the detection of ethanol in petrochemicals,” *IEEE Sensors J.*, vol. 22, no. 13, pp. 12913–12920, Jul. 2022, doi: 10.1109/JSEN.2022.3180205.
- [2] G. Li, Z. Zhou, Z. Wang, S. Chen, J. Liang, X. Yao, and L. Li, “An efficient electrochemical biosensor to determine 1,5-anhydroglucitol with persimmon-tannin-reduced graphene oxide-PtPd nanocomposites,” *Materials*, vol. 16, no. 7, p. 2786, Mar. 2023, doi: 10.3390/ma16072786.
- [3] C. Hong, Q. Yang, W. Chen, S. Yuan, X. Zhao, and X. Ding, “Development of a graphene-based wireless displacement transducer,” *IEEE Sensors J.*, vol. 23, no. 8, pp. 8284–8291, Apr. 2023, doi: 10.1109/JSEN.2023.3255908.
- [4] J. Huang, M. Li, J. Chen, Y. Cheng, Z. Lai, J. Hu, F. Zhou, N. Qu, Y. Liu, and J. Zhu, “Effect of temperatures and graphene on the mechanical properties of the aluminum matrix: A molecular dynamics study,” *Materials*, vol. 16, no. 7, p. 2722, Mar. 2023, doi: 10.3390/ma16072722.
- [5] Q. Yan, Q. Xia, Y. Wang, P. Zhou, and H. Zeng, “URadio: Wideband ultrasound communication for smart home applications,” *IEEE Internet Things J.*, vol. 9, no. 15, pp. 13113–13125, Aug. 2022, doi: 10.1109/JIOT.2021.3139342.

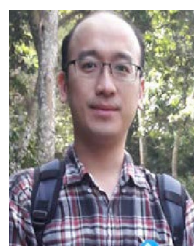
- [6] Z. Liu, M. Zhou, W. Liao, J. Liu, C. Luo, C. Lu, Z. Chen, and H. Zhu, "Fertilizer-holding performance of graphene on soil colloids based on double electric layer theory," *Materials*, vol. 16, no. 7, p. 2578, Mar. 2023, doi: [10.3390/ma16072578](https://doi.org/10.3390/ma16072578).
- [7] A. Mery, Y. Chenavier, C. Marcucci, A. Benayad, J. P. Alper, L. Dubois, C. Haon, N. H. Boime, S. Sadki, and F. Duclairoir, "Toward the improvement of silicon-based composite electrodes via an in-situ Si@C-graphene composite synthesis for Li-ion battery applications," *Materials*, vol. 16, no. 6, p. 2451, Mar. 2023, doi: [10.3390/ma16062451](https://doi.org/10.3390/ma16062451).
- [8] S. Asgari and T. Fabritius, "Graphene-based multiband chiral metamaterial absorbers comprised of square split-ring resonator arrays with different numbers of gaps, and their equivalent circuit model," *IEEE Access*, vol. 10, pp. 63658–63671, 2022, doi: [10.1109/ACCESS.2022.3183272](https://doi.org/10.1109/ACCESS.2022.3183272).
- [9] S. Pawar, H. M. Bernety, and A. B. Yakovlev, "Graphene-metal metasurface for cloaking of cylindrical objects at low-terahertz frequencies," *IEEE Access*, vol. 10, pp. 130200–130211, 2022, doi: [10.1109/ACCESS.2022.3228833](https://doi.org/10.1109/ACCESS.2022.3228833).
- [10] L. Sun, L. Huang, Y. Wang, Y. Lian, G. Huang, H. Zhao, and K. Zheng, "Ultra-low loss graphene plasmonic waveguide for chip-scale terahertz communication," *IEEE Photon. J.*, vol. 13, no. 4, pp. 1–6, Aug. 2021, doi: [10.1109/JPHOT.2021.3097334](https://doi.org/10.1109/JPHOT.2021.3097334).
- [11] G. Li, H. Li, C. Wang, X. Li, J. Chen, J. Liang, and Z. Zhou, "Colorimetric aptasensor for sensitive Glypican-3 detection based on hemin-reduced oxide graphene-platinum@palladium nanoparticles with peroxidase-like activity," *IEEE Sensors J.*, vol. 23, no. 1, pp. 111–118, Jan. 2023, doi: [10.1109/JSEN.2022.3224554](https://doi.org/10.1109/JSEN.2022.3224554).
- [12] B. Nasifowska, W. Skrzeczanowski, A. Bombalska, and Z. Bogdanowicz, "Laser emission spectroscopy of graphene oxide deposited on 316 steel and Ti6Al4V titanium alloy suitable for orthopedics," *Materials*, vol. 16, no. 7, p. 2574, Mar. 2023, doi: [10.3390/ma16072574](https://doi.org/10.3390/ma16072574).
- [13] R. Homsy, N. Al-Azzam, B. Mohammad, and A. Alazzam, "Memristive biosensors for cancer biomarkers detection: A review," *IEEE Access*, vol. 11, pp. 19347–19361, 2023, doi: [10.1109/ACCESS.2023.3248683](https://doi.org/10.1109/ACCESS.2023.3248683).
- [14] A. Maghoul, A. Rostami, M. Veletic, B. D. Unluturk, N. Gnanakulasekaran, and I. Balasingham, "Optical modeling and characterization of demyelinated nerve using graphene-based photonic structure," *IEEE Access*, vol. 10, pp. 28792–28807, 2022, doi: [10.1109/ACCESS.2022.3156113](https://doi.org/10.1109/ACCESS.2022.3156113).
- [15] N.-Q. Deng, W.-J. Liao, J. Hu, P. Wang, M.-X. Xu, H.-N. Zhang, P. Wang, C.-D. Liang, H. Tian, L. Chen, X.-P. Ouyang, Y. Yang, T.-L. Ren, E. X. Zhang, and D. M. Fleetwood, "Total-ionizing-dose effects on a graphene X-ray detector laser-scribed from graphene oxide," *IEEE Trans. Nucl. Sci.*, vol. 65, no. 1, pp. 473–477, Jan. 2018, doi: [10.1109/TNS.2017.2776201](https://doi.org/10.1109/TNS.2017.2776201).
- [16] J.-C. Chou, J.-X. Chang, P.-H. Yang, C.-H. Lai, P.-Y. Kuo, Y.-H. Nien, R.-H. Syu, and P.-F. Cheng, "The application of dy-sensitized solar cell using rGO and MBs in series-parallel under low illumination," *IEEE Access*, vol. 10, pp. 90467–90473, 2022, doi: [10.1109/ACCESS.2022.3202302](https://doi.org/10.1109/ACCESS.2022.3202302).
- [17] B. Alpat, E. Pilicer, S. Blasko, D. Caraffini, F. D. Capua, V. Postolache, G. Saltanocchi, M. Menichelli, L. Desorgher, M. Durante, R. Pleskac, and C. L. Tessa, "Total and partial fragmentation cross-section of 500 MeV/nucleon carbon ions on different target materials," *IEEE Trans. Nucl. Sci.*, vol. 60, no. 6, pp. 4673–4682, Dec. 2013, doi: [10.1109/TNS.2013.2284855](https://doi.org/10.1109/TNS.2013.2284855).
- [18] H. Mu, Y. Gu, and H. Xie, "Photocatalysis of nickel-based graphene/Au/ZnO nanocomposites," *IEEE Sensors J.*, vol. 19, no. 14, pp. 5376–5388, Jul. 2019, doi: [10.1109/JSEN.2019.2907712](https://doi.org/10.1109/JSEN.2019.2907712).
- [19] B. Mazurek, W. Mielcarek, J. Warycha, K. Prociow, J. Chmielowiec, Z. Znamierowski, and E. Popko, "Field emission from graphene produced with use of chemical vapor deposition method," *IEEE Trans. Dielectr. Electr. Insul.*, vol. 22, no. 6, pp. 3498–3504, Dec. 2015, doi: [10.1109/TDEI.2015.005168](https://doi.org/10.1109/TDEI.2015.005168).
- [20] H. Sun, "Graphene nano sheet fabrication using light," *IEEE J. Electron Devices Soc.*, vol. 7, pp. 1094–1099, 2019, doi: [10.1109/JEDS.2019.2948375](https://doi.org/10.1109/JEDS.2019.2948375).
- [21] L. Xia, X. Zhang, D. Wei, H.-L. Cui, and C. Du, "Graphene terahertz amplitude modulation enhanced by square ring resonant structure," *IEEE Photon. J.*, vol. 10, no. 1, pp. 1–7, Feb. 2018, doi: [10.1109/JPHOT.2017.2779870](https://doi.org/10.1109/JPHOT.2017.2779870).
- [22] J. Li, P. Zheng, L. Dong, W. Yang, C. Liu, Y. Yang, Z. Xue, G. Liu, P. Li, and Z. Di, "Centimeter-scale Ge-assisted grown graphene directly on SiO<sub>2</sub>/Si for NO<sub>2</sub> gas sensors," *IEEE Sensors J.*, vol. 21, no. 4, pp. 5164–5172, Feb. 2021, doi: [10.1109/JSEN.2020.3029172](https://doi.org/10.1109/JSEN.2020.3029172).
- [23] M. Xia, H. Shao, Z. Huang, Z. Zhao, F. Jiang, and Y. Hu, "Intelligent process monitoring of laser-induced graphene production with deep transfer learning," *IEEE Trans. Instrum. Meas.*, vol. 71, pp. 1–9, 2022, doi: [10.1109/TIM.2022.3186688](https://doi.org/10.1109/TIM.2022.3186688).
- [24] H. Yu, L. Sun, S. Ji, R. Deng, Z. Mo, and Q. Xie, "Enhanced photoelectric properties of multilayer graphene Mg<sub>2</sub>Si/Si heterojunction photodetector," *IEEE Photon. J.*, vol. 14, no. 1, pp. 1–9, Feb. 2022, doi: [10.1109/JPHOT.2021.3128881](https://doi.org/10.1109/JPHOT.2021.3128881).
- [25] X. Chen, W. Lin, P. Xu, L. Chen, W. Meng, X. Hu, H. Qu, J. Sun, and Y. Cui, "FM-level detection of glucose using a grating based sensor enhanced with graphene oxide," *J. Lightw. Technol.*, vol. 41, no. 13, pp. 4145–4152, Jul. 1, 2023, doi: [10.1109/JLT.2022.3174039](https://doi.org/10.1109/JLT.2022.3174039).
- [26] S. Roy, S. Mondal, and K. Debnath, "Symmetric bound states in the continuum in an all graphene metasurface—Design and sensor applications," *IEEE Sensors J.*, vol. 23, no. 8, pp. 8352–8359, Apr. 2023, doi: [10.1109/JSEN.2023.3252223](https://doi.org/10.1109/JSEN.2023.3252223).
- [27] S. Zhao, H. Ma, M. Jiang, C. Li, Y. Liu, X. Zhao, and X. Chen, "Study of carbon brush and slip-ring system abrasion from electric contact friction under special environments," *IEEE Access*, vol. 9, pp. 9308–9317, 2021, doi: [10.1109/ACCESS.2021.3050098](https://doi.org/10.1109/ACCESS.2021.3050098).
- [28] L.-Y. Huang, H.-D. Liu, S.-D. Lu, and C.-M. Hsu, "Novel graphene allocating carbon-copper ratio method for the rail vehicle propulsion system ground carbon brush," *IEEE Access*, vol. 10, pp. 52890–52898, 2022, doi: [10.1109/ACCESS.2022.3174572](https://doi.org/10.1109/ACCESS.2022.3174572).
- [29] D. H. Park, J. Kwak, Y.-S. Kim, H. Lee, Y. Lee, Y.-J. Kim, B. Han, and H.-J. Kim, "A study on the particle removal efficiency and durability according to the material of the ionizer of the fiber brush type electric precipitator," *IEEE Trans. Ind. Appl.*, vol. 59, no. 1, pp. 486–491, Jan. 2023, doi: [10.1109/TIA.2022.3217743](https://doi.org/10.1109/TIA.2022.3217743).



**LIANG-YIN HUANG** received the M.S. degree from the National Taipei University of Technology (NTUT), Taipei, Taiwan, in 2015, and the Ph.D. degree from the Graduate Institute of Manufacturing Technology, NTUT, in 2023. From January 1999 to January 2023, he was a Group Chief with Metro Taipei. Since February 2023, he has been a Senior Engineer with New Taipei Metro Corporation. His primary research interests include materials engineering, rail vehicles, and solar energy engineering.



**SHIUE-DER LU** (Member, IEEE) received the M.S. degree in electrical engineering from Chung Yuan Christian University (CYCU), in 2006, and the Ph.D. degree in electrical engineering from the National Taiwan University of Science and Technology (NTUST), in 2013. Since 2018, he has been with the Department of Electrical Engineering, National Chin-Yi University of Technology (NCUT), where he is currently an Associate Professor. His research interests include renewable energy, power systems, fault diagnosis, and optimization algorithm.



**HWA-DONG LIU** received the M.S. degree from Chung Yuan Christian University, Taoyuan, Taiwan, in 2006, and the Ph.D. degree from the National Taiwan University of Science and Technology, Taipei, Taiwan, in 2020. From April 2008 to July 2021, he was a Group Chief with Metro Taipei. Since August 2021, he has been with the Undergraduate Program of Vehicle and Energy Engineering, National Taiwan Normal University, Taipei, where he is currently an Assistant Professor. His primary research interests include power electronics for electric vehicle applications and solar energy.

• • •